

Creation of the first UXO detection test site in Slovakia at the Rohožník military training range

Roman PAŠTEKA^{1,*} , Roland KARCOL¹ , David KUŠNIRÁK¹ ,
Ema NOGOVÁ² , Erik ANDRÁSSY¹ 

¹ Department of Engineering Geology, Hydrogeology and Applied Geophysics,
Faculty of Sciences, Comenius University, Ilkovičova 6, 842 15 Bratislava, Slovak Republic

² Earth Science Institute Slovak Academy of Sciences,
Dúbravská cesta 9, P.O. Box 106, 840 05 Bratislava, Slovak Republic

Abstract: In the development of geophysical methods for unexploded ordnance detection, a very important role is played by UXO test sites, where known ordnance and other explosive/nonexplosive items are buried in the ground at defined positions. At such sites, various detection methods can be compared, developed and tested. Based on a cooperation between the Department of Applied Geophysics (Comenius University), Institute of Forensic Science (Slovak Ministry of Interior) and Rohožník military training range a project was performed, which was focused on the creation of the first UXO detection test site in Slovakia. It was restricted to one type of ordnance – inert tank projectiles with diameter of 100 mm. These were buried in the ground at different depths and with different orientations. Data acquisition mapping the test site was performed from the ground surface, using total field intensity magnetometers, vertical difference magnetometers and ground penetrating radar (GPR). Data acquired from all methods were processed, interpreted and archived for future reference. Most of the items were readily detected by each of the detection sensors used but the deepest items at the least favourable orientation exceeded the detection limit of the magnetometers trialled with total field performing better than the vertical gradiometers. For the application of GPR, this site was found to have favourable soil conductivity conditions permitting even the deepest items to be detected when favourably oriented. Vertical orientation presenting the smallest reflective cross-section was least favourable with some shallow items escaping detection. The most accurate depth estimations for detectable items were obtained from GPR data presented as 2D non-migrated vertical sections. Geophysical data sets acquired at seeded test sites such as the one now established at the Rohožník military training range can provide important base-line data for comparison from which the development of new detection and data interpretation technologies can be evaluated.

Key words: UXO, test-site, magnetometry, GPR

*corresponding author, e-mail: pasteka@fns.uniba.sk

1. Introduction

It is commonly known that geophysical sensing methods are very important in their application to UXO detection and discrimination (UXO = UneXploded Ordnance). Among them, the most useful are magnetic and electromagnetic methods. These methods were introduced and developed by many authors (e.g. *Butler, 2001; Stanley and Cattach, 2004*). There exist many successful applications of high-definition magnetics and electromagnetic methods (e.g. *Billings and Youmans, 2007*), but there is still need for new developments in acquisition, processing and interpretation techniques (e.g. *Gasperikova et al., 2009; Ibraheem et al., 2021*). To the knowledge of authors, shallow seismic methods have not been successfully used for UXO detection, although they do have excellent characteristics suited to some near surface applications (e.g. *Steeple, 2000; Brixová et al., 2018*).

An important role is played by UXO test sites, where known ordnance and other explosive/nonexplosive items are buried in the ground at defined positions and orientations where developments in methods for their detection can be tested. Among them the “Jefferson Proving Ground” in Indiana has become the best known and mostly widely used (e.g. *Curtis, 1999; Robitaille et al., 1999*). This was established by the US Army Corps of Engineers in 1993 for a large scale comparison of UXO detection techniques in the US. There are also sites in the hands of private companies, used for internal reasons, but sometimes open also for other experts in a frame of workshops and exhibitions (e.g. *NSGG UXO Test site, 2023*, managed by Geomatrix Earth Science Ltd.).

Based on a cooperation between the Department of Applied Geophysics (Comenius University), Institute of Forensic Science (Slovak Ministry of Interior) and Rohožník military training range a project was performed, which was focused on the creation of the first UXO detection test site in Slovakia – located at the Rohožník military training site. This site was seeded with just one type of ordnance, with items buried at different orientations and different depths as shown in Fig. 1. The depth of the deepest ordnance was selected to challenge the capability of current state-of-the-art technologies. The ordnance selected was an inert tank projectile of diameter 100 mm and length 500 mm.

Initial base-line data mapping the test site was acquired using two different geophysical principles and involved the use of two different sensor

types. Magnetic data were acquired using a total field magnetic sensor (Cs-vapour atomic sensor) and vertical difference measurements between vertical component magnetic sensors (fluxgate) of two different sensor separations. Ground Penetrating Radar (GPR) data was also acquired, mapping this site. These data sets were then processed, interpreted and archived for future reference.

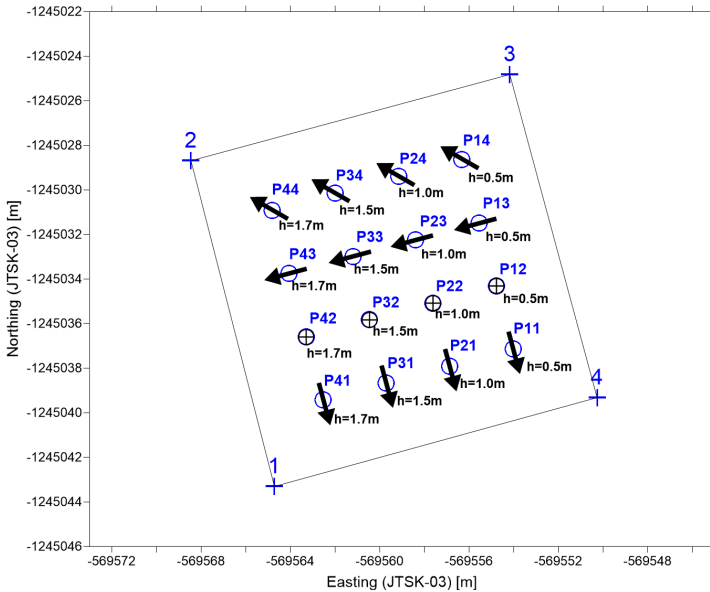


Fig. 1. Position and orientation of 16 inert tank projectiles (P11–P14, P21–P24, P31–P34, P41–P44) with diameter of 100 mm within the test site. Arrows show the orientation of projectiles. Those in the second line from the bottom point upwards in the vertical direction. Values in the figure show the depths of projectiles centres from the surface.

2. Preparation and creation of the UXO test site

Thanks to an outstanding cooperation between the Department of Applied Geophysics (Comenius University), Institute of Forensic Science (Slovak Ministry of Interior. Lt. Juraj Kadecký) and Rohožník military training range (sergt. Ján Jaráb) a small area measuring 15×15 m was dedicated for the establishment of a UXO test site. Within this area 16 items of inert tank projectiles with diameter of 100 mm were buried in a regular grid

pattern of 3×3 m. The position, orientation and depth of these items are shown in Fig. 1. In addition to these control items, samples of a smaller 85 mm projectile and BDU-33 practice bomb of 100 mm diameter were placed on the ground surface along the eastern edge of the site. The UXO types used at the site are shown in Fig. 2.

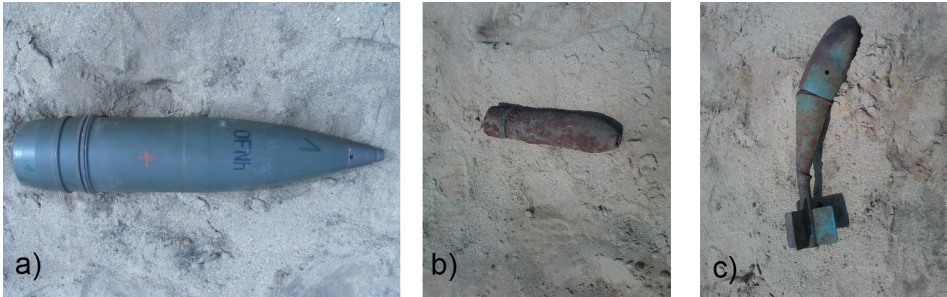


Fig. 2. a) Inert tank projectiles with diameter of 100 mm used as the main object of testing; b) Smaller tank projectile of diameter 85 mm; c) An inert BDU-33 areal practice bomb of diameter 100 mm.

As can be seen in Fig. 3, the ground at his site consisted of a thick layer of sand with very low volume magnetic susceptibility and very low electric conductivity. This environment is most favourable for the detection of UXO using geophysical methods. The geodetic coordinates of the test site cor-



Fig. 3. The execution of digging on the new test site in sandy soil conditions. This important part of the project was performed by the experts from the Institute of Forensic Science, Slovak Ministry of Interior.

ners (1, 2, 3, 4, Fig. 1) were determined by means of the GNSS instrument Trimble R8s using the real-time service SKPOS.

Inert tank projectiles were identified by a sequence numbers P11–P14, P21–P24, P31–P34 and P41–P44 as shown in Fig. 1. Projectiles were oriented with respect to magnetic north and were put in horizontal or vertical positions as indicated. The projectiles were placed at different depths ranging from 0.5 m (P11–P14), 1.0 m (P21–P24), 1.5 m (P31–P34) and 1.7 m (P41–P44). Projectiles P14, P24, P34, P44 were in a horizontal position with the orientation approximately to NW. Projectiles P13, P23, P33, P43 were also in a horizontal position but oriented approximately WSW. Projectiles P12, P22, P32, P42 were placed vertically pointing from bottom to the top. Projectiles P11, P21, P31, P41 were again in horizontal position with the orientation approximately to SSE. The exact geodetic coordinates of all 16 projectiles in the system JTSK-03 were determined by means of the GNSS instrument Trimble R8s and were archived for future comparisons and studies.

3. Geophysical measurements at the new UXO test site

After the creation of the test site, several initial geophysical measurements were acquired using different methods and instruments:

- total field magnetometer with 1 hand-held Cs-vapour sensor (instrument TM-4),
- magnetometric vertical component, vertical difference over a 650 mm separation gradiometry with 5 fluxgate sensors on a cart (instrument SENSYS MXPDA),
- magnetometric vertical component, vertical difference gradiometry over a 400 mm separation with 1 hand-held fluxgate sensor (instrument SENSYS SBL10),
- ground penetrating radar (instrument GSSI SIR-3000 with 400 MHz antenna).

Of the methods used, the array of vertical component gradiometer sensors mounted on a hand operated cart magnetometry was the fastest, Fig. 4. The slowest was the GPR but at this site it provided the benefit of greatest

accuracy in target depth measurement. Prior to conducting the magnetometric measurements, we positioned along the eastern edge of the test site few additional UXO objects (Fig. 2b,c) on the surface. The aim in doing this was to also obtain responses from very shallow objects.



Fig. 4. Data acquisition with SENSYS MXPDA magnetometer (with 5 vertical component fluxgate gradiometer sensors and GNSS Trimble R8s receiver) on a hand operated cart.

4. Data acquisition and processing

A. Total field magnetometer (TM-4 with 1 sensor)

A TM-4 magnetometer (GTL Armidale, Australia) was used together with one Cs-vapour total field sensor model G822AS from the company Geometrics, USA. This magnetometer system is regarded as the best instrument of this category worldwide. Sampling can be determined at 400 Hz with a resolution of ± 0.1 nT and absolute precision ± 1 nT. With this specification the received signal is usually of a very good quality and well sampled. Distance between acquisition lines was 0.5 m, with sampling along line at 0.1 m intervals. Data acquisition was performed in local coordinates and the position along acquisition lines was determined by means of an optical, cotton thread odometer. After data acquisition, measured values were transferred to a computer. A median filter with the window length of 100

points was applied to the data from each measured line to remove diurnal drift and the final values were then interpolated into a 0.2×0.2 m grid. The anomalous total magnetic induction field was then visualised in the form of a coloured image (Fig. 5), where the map itself was georeferenced in the JTSK03 coordinate system.

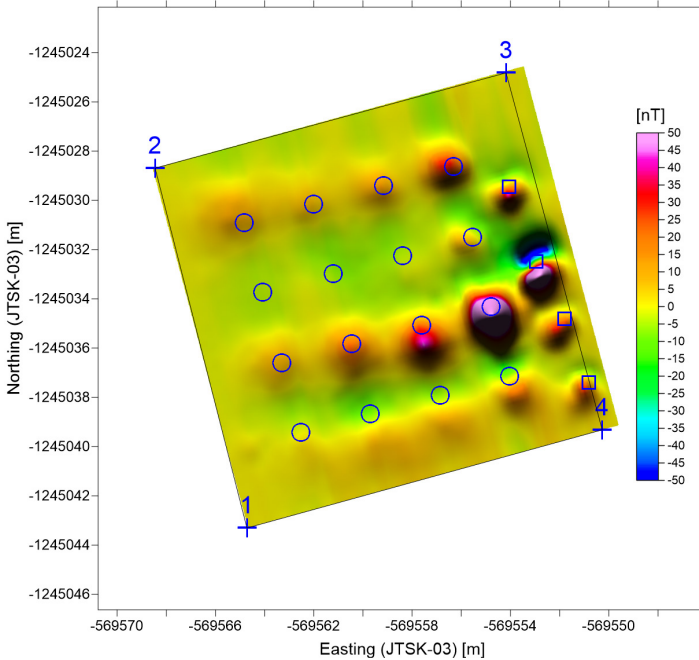


Fig. 5. The anomalous total magnetic induction field (instrument TM-4). Blue circles show the centres of 16 buried projectiles, blue squares are the centres of additional projectiles, which were positioned on the surface.

B. Vertical difference, vertical magnetic component (MXPDA with 5 sensors)

The fluxgate magnetometer array from SENSYS model MXPDA (Sensys GmbH, Bad Saarow, Germany) operates with 5 vertical component, vertical difference sensors type FGM650 (Fig. 4), each consisting of a pair of fluxgate sensor elements separated vertically by 650 mm. The across-line separation distance was 0.5 m and the sampling interval along-line was 0.1 m. Sen-

sensor resolution was approximately ± 0.2 nT. Determination of the position in the global coordinate system (ETRS89) was performed by means of the GNSS Trimble RS8 system, using the service SKPOS. After data acquisition, measured values were transferred to a computer, median filtered with the window length of 100 points and final values were interpolated into a 0.2×0.2 m grid. The anomalous difference in the vertical component of the magnetic field was visualised in a form of coloured image (Fig. 6) directly in the JTSK03 coordinate system.

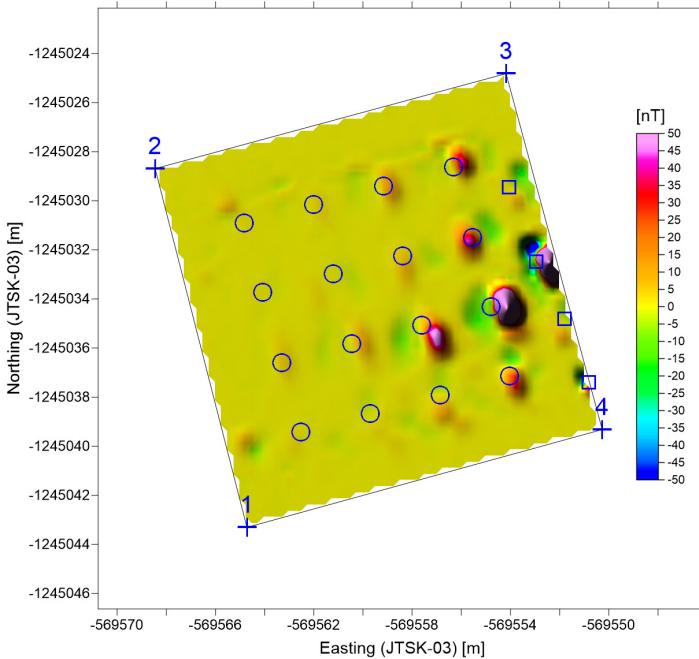


Fig. 6. The anomalous vertical difference between vertical component magnetic sensors separated by 650 mm (instrument SENSYS MXPDA). Blue circles show the centres of 16 buried projectiles, blue squares are the centres of additional projectiles, which were positioned on the surface.

C. Vertical difference, vertical magnetic component (SBL10 with 1 sensor)

The fluxgate magnetometer SENSYS model SBL10 (Sensys GmbH, Bad Saarow, Germany) operates with 1 vertical component, vertical difference

sensor consisting of a pair of fluxgate sensor elements type FGM400 separated vertically by 400 mm. Results were acquired in a local coordinate system. The position of samples along walking lines was interpolated assuming a constant walking speed. The resulting difference field from the SBL10 is displayed in Fig. 7.

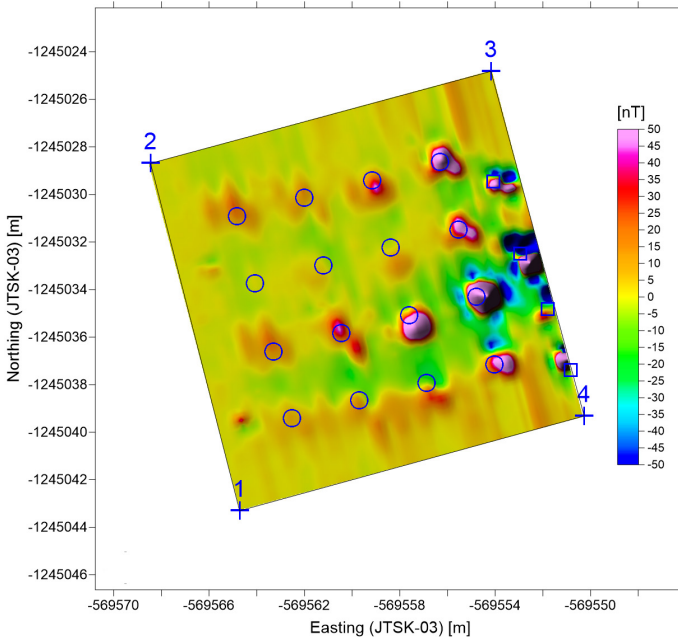


Fig. 7. The anomalous field of vertical difference between vertical component magnetic sensors separated by 400 mm (instrument SENSYS SBL10). Blue circles show the centres of 16 buried projectiles, blue squares are the centres of additional projectiles, which were positioned on the surface.

D. Ground penetrating radar (GSSI with 400 MHz antenna)

Measurements by means of the GPR method were performed using a system from GSSI (Geophysical Survey Systems Inc, Nashua NH, USA) with the model SIR-3000 control unit and a 400 MHz antenna. The distance between acquisition lines was 0.15 m, this being half the antenna width. Reflection amplitude data sampled with 1024 points over a 100 ns period was recorded at 2 cm intervals along line. Acquired data were processed by means of

the software REFLEXW (Sandmeier, 2019). In the first processing step, 2D vertical radargrams were processed, applying start time removal, mean value filtering, interpolation and band-pass filtering (200/650 MHz). In the next steps a gain function was applied for amplification of reflection amplitudes (Figs. 8–11). In a supplementary processing stage, reflection amplitudes were interpolated into a 3D volume and horizontal slices for different penetration depths were then produced (Figs. 12–13).

5. Visualisation of results

The results of magnetic data acquisition have been presented as images where the signal amplitude is mapped in linear scaled colour contours. The total field data was represented in Fig. 5, the vertical component difference data acquired with 650 mm vertical sensor separation was presented in Fig. 6 and the vertical component difference data acquired with 400 mm vertical sensor separation was presented in Fig 7.

The GPR data has been presented in two formats. Figures 8 to 11 show vertical two way travel time reflection images for sections directly above

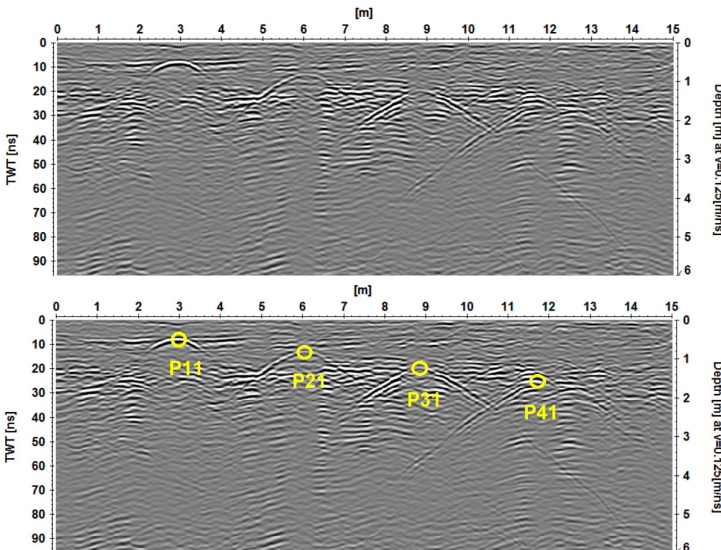


Fig. 8. Original (top) and interpreted (bottom) 2D vertical radargram with detected diffraction waves from objects P11–P41.

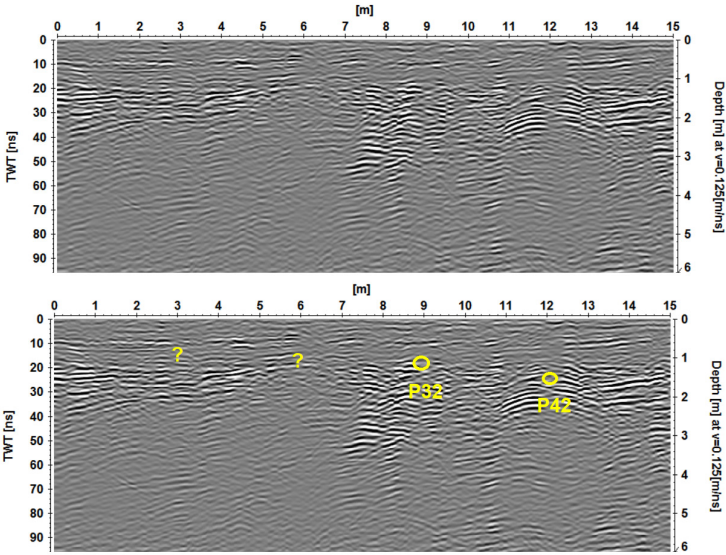


Fig. 9. Original (top) and interpreted (bottom) 2D vertical radargram with detected diffraction waves from vertically oriented objects P32 and P42 (objects P12 and P22 could not be detected – diffraction waves were not well developed).

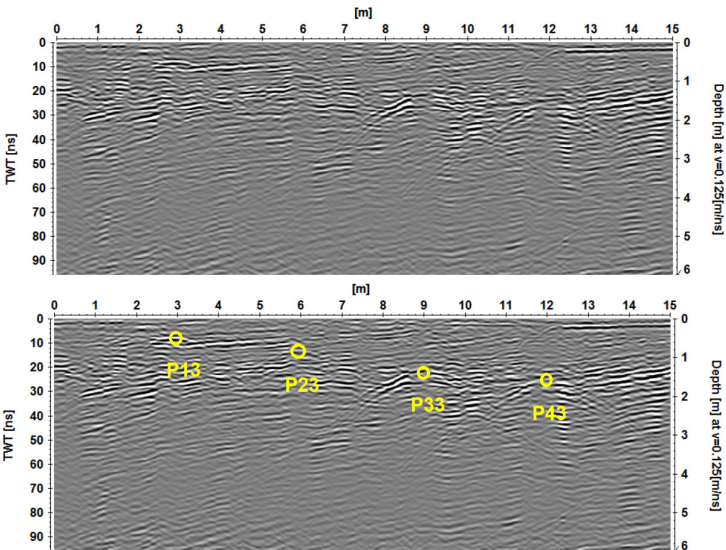


Fig. 10. Original (top) and interpreted (bottom) 2D vertical radargram with detected diffraction waves from objects P13–P43.

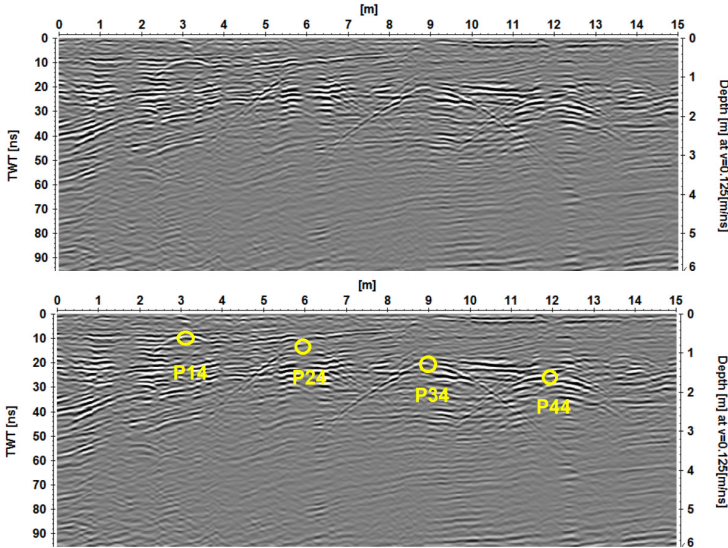


Fig. 11. Original (top) and interpreted (bottom) 2D vertical radargram with detected diffraction waves from objects P14–P44.

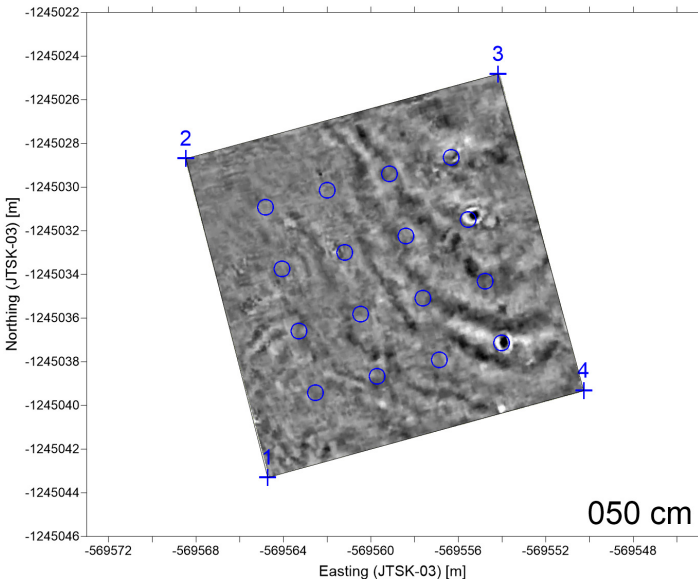


Fig. 12. Selected typical horizontal GPR amplitude slice for interpolation depth below the surface of 50 cm.

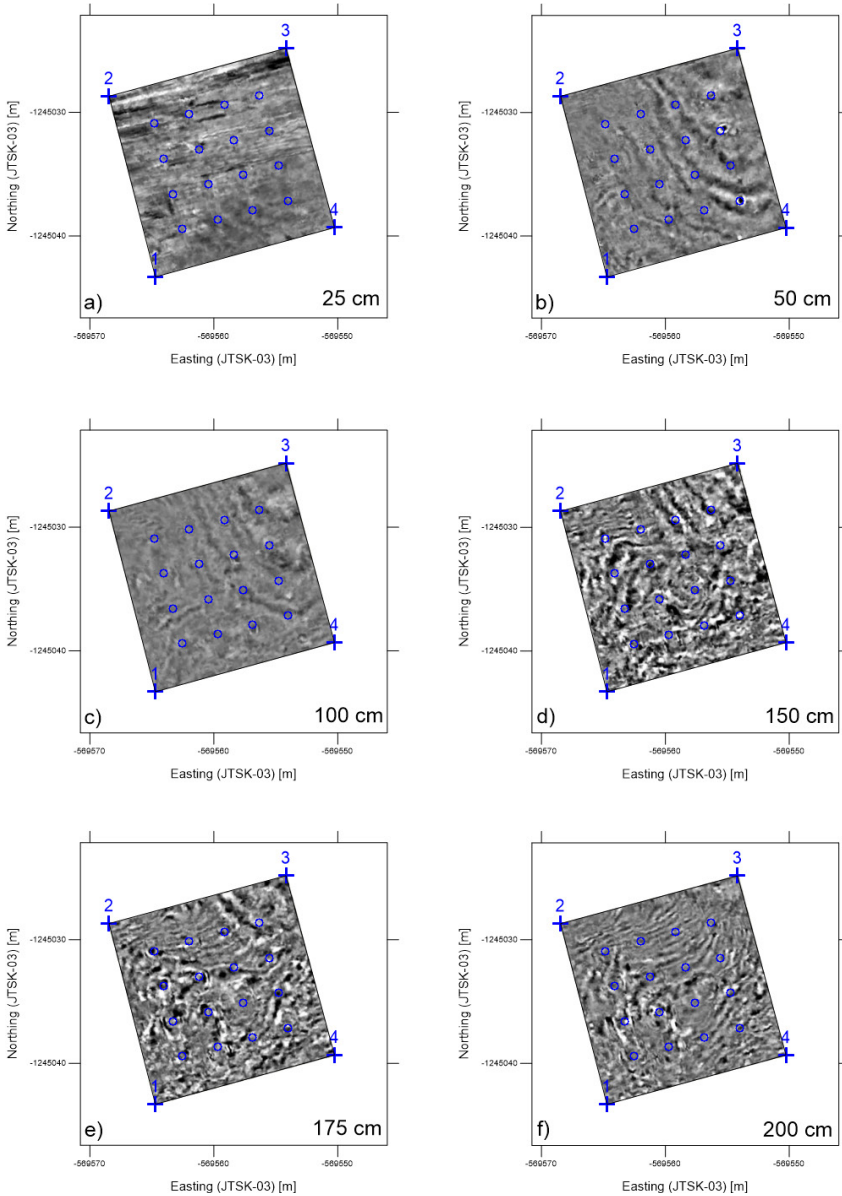


Fig. 13. Selected horizontal GPR amplitude slices for interpolation depths below the surface: a) 25 cm, b) 50 cm, c) 100 cm, d) 150 cm, e) 175 cm, f) 200 cm.

each of the four lines of buried targets. In these images the reflection from a UXO item is recognised as an hyperbolic pattern (diffraction waves), the top of which was located directly above the target. An alternate presentation of the GPR was in the form of horizontal sections at different depths. Figure 12 shows in detail such a section from 0.5 m depth. Superimposed on this image is the location of the buried UXO. In this case, horizontally oriented UXO at 0.5 m depth can be clearly identified although the vertical item presenting a much smaller reflecting surface area cannot be seen. Figure 13 contains horizontal sections from depths of 0.25, 0.5, 1.0, 1.5, 1.75 and 2.0 metres.

6. Interpretation of obtained results and discussion

The results from the acquired geophysical fields were informative in that they exposed the strengths and weaknesses of each detection and processing system used.

A. Total field magnetic data

It was verified that the amplitude of each anomaly was significantly dependent upon the resultant magnetisation of the object (with strong influence of its remanent component) its orientation and its depth (*Pašteka et al., 2010*, among others). Only two of the items were not readily detected from the total field data. The two projectiles P33 and P43 displayed anomalies with very low amplitudes that were at the detectable limit by means of total field magnetometry. The response from P33, the shallower of the two could easily have been overlooked, but the signal detected was able to be interpreted. The low amplitude response was due to a combination of depth with an orientation least favourable at this latitude. The vertically oriented projectiles P12–P22–P32–P42 resulted in anomalies with relatively high amplitudes (Figs. 5, 6 and 7), which is partly influenced by the fact that the upper edges of these projectiles are approximately 15–20 cm closer to the surface, when compared to projectiles in horizontal positions. The magnetic field associated with these items was also favoured by their long axis more closely paralleling the Earth’s magnetic field in this latitude.

B. 650 mm vertical difference, vertical component magnetometry

The vertical difference data recorded from sensors separated by 650 mm was able to detect all items buried 1 m or less regardless of orientation. It was also able to detect the most favourably oriented, vertical items even to 1.7 m depth. With the sensor separation of 650 mm this “difference” measurement only partially approximates a gradient for the shallow objects. For the deeper items the approximation to a gradient is much closer. It is well understood that while the total field response from a dipole drops off approximately as an inverse square of the depth, the gradient reduces by the inverse 3rd power. This explains the easier detection of deeper items observed using total field measurement.

C. 400 mm vertical difference, vertical component magnetometry

The vertical difference data recorded from sensors separated by 400 mm more closely reflects the vertical gradient. All items within 1 m of the surface were still able to be detected as were the vertically oriented UXO even at 1.7 m. But the less favourably oriented items deeper than 1 m were not reliably detected. This degrading of the detection ability of a 400 mm difference sensor, reflects its closer approximation to gradient measurement with the associated loss of signal amplitude. The data shown in Fig. 7 also reveals the poorer position measurement accuracy achieved when relying upon the operator walking at constant velocity.

D. Ground penetrating radar

The low conductivity soil at this site enabled very favourable results to be obtained using the GPR method (GSSI with 400 MHz antenna). As it can be seen in processed 2D vertical sections (Figs. 8–11), all but two of the buried objects are manifested by intensive diffraction waves (with hyperbolic shape), which is typical behaviour of isolated reflective sources in the GPR wavefield. For the depth estimation, the top of each diffraction wave was taken as the depth of the object (its upper edge).

The two items that could not be detected by GPR (P12 and P22, Fig. 9) were both vertically oriented with the sharp end pointing upwards. This

geometry reflected the radar energy side-ways and down-wards with minimal energy returning to the ground surface. As we observed, the vertical orientation favours magnetic detection and this provides a nice example of the situation, when two geophysical methods can complement each other.

In the interpolated horizontal slices for different penetration depths (Figs. 12 and 13), the presence of buried objects can in general be hardly seen, best results were achieved for the shallower depths (e.g. 50 cm in Fig. 12). In this horizontal section we can even recognise the orientation of some of the projectiles (e.g. P11 and P13). But for larger penetration depths pedological/geological features are more visible and these become dominant and mask the anomalies from searched objects. Maybe there is scope in the future for developing improved migration procedures that could improve this kind of visualisation. From this experience the interpretation of GPR data (for this application) in 2D non-migrated vertical sections with amplified amplitudes remains preferred.

These good results from the GPR method were obtainable due to the very favourable physical properties of the soils (sands), where the objects were buried. The low values of electrical conductivity and permittivity are ideal for the use of GPR. The application of the GPR method in more complicated environments can bring quite complicate results for interpretation, as several authors comment on a strong attenuation of diffraction hyperbolas due to unwelcome soil conditions (e.g. *Arcone et al., 2000*).

While detection is the primary objective in the search for buried UXO, interpretation of the data in terms of the size, depth and position of the source and discrimination against non UXO items that may be present are of paramount importance. At this site there are no clutter items and so it is not suitable for discrimination studies.

In this investigation, quantitative interpretation (dipole fitting and Euler deconvolution) was applied only to the total field magnetometric data as these estimation methods have not yet been adapted for the outputs from vertical component, vertical difference sensors. But anomalous fields from the vertical difference data (Figs. 6 and 7) from shallow items closely resembles total field data in appearance.

As already presented by *Pašteka et al. (2021)*, we also have used two independent methods for the depth determination of the objects from the total field data. The first uses the optimisation approach (*Marquardt, 1963*)

in fitting magnetic dipole or ellipsoid in the depth of the interpreted anomaly (software MAGSYS). The second one is 3D Euler deconvolution (*Reid et al., 1990*) with incorporation of so-called regularized derivatives (*Pašteka et al., 2009*) (software REGDER). The results are summarized in Table 1, where we can see that MAGSYS software provided much more reliable results than did Euler deconvolution. It was noted that MAGSYS tended to slightly underestimate the depth to the deeper items. Only in the case of the very low anomaly amplitude signal from object P43 could the method not be applied (this anomaly was very weak and influenced by other surrounding effects). In the case of 3D Euler deconvolution there were more cases (objects: P31, P41, P23, P33, P43, P34), where the method failed – no clusters of depth solutions were obtained in these cases.

The quantitative interpretation of the GPR data required knowledge of the radar velocity in the soil conditions encountered. Velocity of the electromagnetic waves was estimated by means of the approximation of diffraction

Table 1. Real and estimated depths of all buried projectiles (N/A – Not Applicable).

projectile #	orientation	true depth [m]	dipole fitting estim. depth [m]	Euler deco estim. depth [m]	2D georadar estim. depth [m]
P11	horiz.	0.5	0.5	0.6	0.5
P21	horiz.	1.0	0.9	1.1	0.9
P31	horiz.	1.5	1.2	N/A	1.5
P41	horiz.	1.7	1.3	N/A	1.7
P12	vert.	0.5	0.5	0.55	N/A
P22	vert.	1.0	0.9	0.9	N/A
P32	vert.	1.5	1.3	1,2	1.4
P42	vert.	1.7	1.3	1.3	1.6
P13	horiz.	0.5	0.5	0.6	0.5
P23	horiz.	1.0	0.85	N/A	1.0
P33	horiz.	1.5	1.2	N/A	1.5
P43	horiz.	1.7	N/A	N/A	1.7
P14	horiz.	0.5	0.5	0.6	0.5
P24	horiz.	1.0	0.9	0.9	1.0
P34	horiz.	1.5	1.3	N/A	1.5
P44	horiz.	1.7	1.3	1.3	1.7

hyperbolas resulting in a value of 0.125 m/ns. This value was used for the calculation of depths of detected objects from the TWT (two-way-time) value. The most accurate depth estimations for detectable items were obtained at this site from GPR data presented as 2D non-migrated vertical sections. As can be seen in Table 1, the quantitative interpretation of the GPR data delivered the most accurate results for all of the items able to be detected. In the case of vertically oriented projectiles P32 and P42 (Fig. 9) the estimated depth of the objects was measured 10–15 cm shallower than the depth to the centre of the object. This was because the waves were reflected from the top part of the projectile which is shallower than the centre of the object when it is positioned in vertical orientation.

7. Conclusions and outlooks

In the presented paper we report on the creation of the first UXO detection test site in Slovakia, located at the Rohožník military training site. This site accommodates 16 projectiles with 100 mm diameter in different orientations, buried in various depths (0.5 m, 1.0 m, 1.5 m, 1.7 m) at locations on a 3×3 m grid. Positions of the site corners and the location of buried projectiles were precisely determined by GNSS technology, with an accuracy of few centimetres. We also documented and archived base-line data sets acquired at this site using total field magnetic detection, two vertical difference, vertical component detectors commonly used in UXO detection, and GPR. The best combination for reliable and precise detection of these projectiles and their depth estimation was the interpretation of mapped total magnetic field data and GPR results presented in 2D, non-migrated vertical sections with amplitude amplification. The total field data (instrument TM-4) revealed all but the deepest, least favourably oriented item. The vertical difference, vertical component sensors (instruments SENSYS MXPDA and SBL10) could detect all projectiles 1 m deep or less but only the more favourably oriented deeper items. The SBL10 with less separation between the component sensors (400 mm instead of 650 for the MXPDA) more closely resembled a gradiometer and consequently was less able to detect the deeper items. The GPR method (instrument GSSI SIR-3000 with 400 MHz antenna) could detect all objects except two shallow projectiles at 0.5 m depth that were oriented vertically with the pointed end facing

upwards thereby deflecting the GPR signal sideways with minimal energy returning to the surface. On those items detected by GPR, this data provided the most accurate depth measurement.

One perceived limitation of our new test site was the relative closeness of buried objects horizontally (3×3 m). This caused some interference (overlapping) of magnetic anomalies from adjacent projectiles. On the other hand, this fact can be in some situations an advantage, for example when studying the performance of detection methods in cluttered situations, where several UXO objects are positioned close to each other. Such situations occur in real world applications and deserve a specifically designed test site.

The new test site will be helpful in the future for comparing and testing new acquisition methods and interpretation techniques against this baseline of current state-of-the-art magnetic and GPR technologies. We need next to add to this baseline, data from current state-of-the-art, 3-component EM instruments and digital metal detectors. In the future we plan also to test different GPR systems, new kinds of magnetic field transformations (based on ratios of numerical derivatives) and we also plan to migrate the GPR data for the enhancement of 3-D visualisation.

Acknowledgements. The presented work was supported by the scientific program of the Ministry of Interior of Slovak Republic PPZ-OAI1-2021/004009-092 and partly also by the project of the Scientific and Grant Agency of Slovak Republic VEGA 2/0100/20. It is important to express our thanks to the military and technicians of the Rohožník military training range. Such a project could be performed only thanks to their enormous technical support. Great thanks belong also to John Stanley for the help with English language editing and important suggestions regarding the structure of manuscript.

References

- Arcone S. A., O'Neill K., Delaney A. J., Sellmann P. V., 2000: UXO Detection at Jefferson Proving Ground using ground-penetrating radar. Report ADA378501, Defense Technical Information Center, 37 p.
- Billings S., Youmans C., 2007: Experiences with unexploded ordnance discrimination using magnetometry at a live-site in Montana. *J. Appl. Geophys.*, **61**, 3-4, 194–205, doi: 10.1016/j.jappgeo.2006.05.008.
- Brixová B., Mosná A., Putiška R., 2018: Applications of shallow seismic refraction measurements in the Western Carpathians (Slovakia): Case studies. *Contrib. Geophys. Geod.*, **48**, 1, 1–21, doi: 10.2478/congeo-2018-0001.

- Butler D. K., 2001: Potential fields methods for location of unexploded ordnance. *Lead. Edge*, **20**, 8, 890–895, doi: 10.1190/1.1487302.
- Curtis J. O., 1999: An Overview of Jefferson Proving Ground UXO Technology Demonstration (Phase III). Technical Report EL-99-12, U.S. Army Environmental Center and U.S. Army Corps of Engineers, Wahsington DC.
- Gasperikova E., Smith J. T., Morrison H. F., Becker A., Kappler K., 2009: UXO detection and identification based on intrinsic target polarizabilities — A case history. *Geophysics*, **74**, 1, B1–B8, doi: 10.1190/1.2997419.
- Ibraheem I. M., Aladad H., 2, Alnaser M. F., Stephenson R., 2021: IAS: A new novel phase-based filter for detection of unexploded ordnances. *Remote Sens.*, **13**, 21, 4345, doi: 10.3390/rs13214345.
- Marquardt D. W., 1963: An algorithm for least squares estimation of nonlinear parameters. *J. Soc. Ind. Appl. Math.*, **11**, 2, 431–441, <http://www.jstor.org/stable/2098941>.
- NSGG UXO Test Site, Geomatrix Earth Science Ltd., 2023: The Superconducting Gravimeter. Available online (accessed on January 27th 2023): <https://www.geomatrix.co.uk/tools/nsgg-uxo-test-site/>.
- Pašteka R., Richter F. P., Karcol R., Brazda K., Hajach M., 2009: Regularized derivatives of potential fields and their role in semi-automated interpretation methods. *Geophys. Prospect.*, **57**, 4, 507–516, doi: 10.1111/j.1365-2478.2008.00780.x.
- Pašteka R., Karcol R., Mikuška J., 2010: Study of the differences between fired and non-fired ordnance ased on their magnetisation. Final report, G-trend, s.r.o., archive, 32 p. (in Slovak).
- Pašteka R., Hajach M., Brixová B., Mikuška J., Stanley J., 2021: Real magnetic stripping method in unexploded ordnance detection and remediation – a case study from Rohožník military training range in SW Slovakia. *Contrib. Geophys. Geod.*, **51**, 3, 277–294, doi: 10.31577/congeo.2021.51.3.5.
- Reid A. B., Allsop J. M., Granser H., Millet A. J., Somerton I. W., 1990: Magnetic interpretation in three dimensions using Euler deconvolution. *Geophysics*, **55**, 1, 80–91, doi: 10.1190/1.1442774.
- Robitaille G., Adams J., O’Donnell C., Pope B., 1999: Jefferson Proving Ground technology demonstration program summary. Army Environmental Center Report Number: SFIM-AEC-ET-TR-99030, 20 p.
- Sandmeier K. J., 2019: ReflexW Vers. 9, Manual. SandmeierGeo, Karlsruhe, Manuscript, online, accessed 2019-11-18, available at: <https://www.sandmeier-geo.de/download.html>.
- Stanley J. M., Cattach M. K., 2004: Developing geophysical techniques for detecting unexploded ordnance. *First Break*, **22**, 9, 41–46, doi: 10.3997/1365-2397.22.9.26015.
- Steeple D. W., 2000: A review of shallow seismic methods. *Ann. Geofis.*, **43**, 6, 1021–1044, doi: 10.4401/ag-3687.